11176-H101-R0-00

APOLLO LM AND CSM S-BAND ANTENNA TRACKING STUDIES
TASK E-53C-1
TECHNICAL REPORT

NAS9-8166

18 December 1968

CSM-HGA INTERCHANGEABILITY STUDY
ERROR ANALYSIS OF THE MONOPULSE COMPARATORS

Prepared For

NATIONAL AERONAUTICS AND SPACE ADMINISTRATION
MANNED SPACECRAFT CENTER
HOUSTON, TEXAS

TRW SYSTEMS GROUP

11176-H101-R0-00

APOLLO LM AND CSM S-BAND ANTENNA TRACKING STUDIES

CSM-HGA INTERCHANGEABILITY STUDY
ERROR ANALYSIS OF THE MONOPULSE COMPARATORS
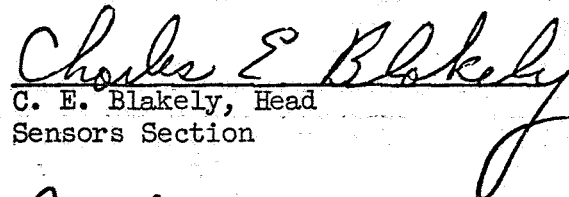
TASK E-53C-1

Prepared by

Robert L. Fogel

18 December 1968

Approved by: *Jack W. Pool*
Jack W. Pool, Manager
TRW Task E-53C-1

Approved by: *Charles E Blakely*
C. E. Blakely, Head
Sensors Section

Approved by: *John DeVillier*
J. DeVillier, Manager
Communications and Sensor Systems
Department

TRW
SYSTEMS GROUP

TABLE OF CONTENTS

LIST OF FIGURES

1.0 INTRODUCTION

1.1 PURPOSE

This report contains an analysis of the narrow beam and wide beam comparators used in the CSM High Gain Antenna Tracking System. The analysis is in support of the CSM High Gain Antenna Interchangeability Study on Task E-53C-1, and its purpose is to determine the errors in the comparators caused by tolerance build-up during manufacturing and assembly and by temperature effects on the comparators. These errors are then used in the system mathematical model to determine their effect on the system transfer function and thus upon interchangeability.

1.2 PROCEDURE

The heart of both the narrow beam and wide beam comparator circuitry, which is shown in Figure 1, is the hybrid ring which is used to take the vector sum and difference of two coherent input signals.

The first step is to analyze the performance of a hybrid ring with one input signal at a port which corresponds to one of the antenna ports. The analysis is repeated for a single input at a second port which corresponds to the second antenna port. The results of these analyses are expressions for the output signals at all ports with an input signal at one port. Since the hybrid is a linear device, the principle of super-position can be used to calculate the output of all arms when the hybrid has coherent signal inputs at two ports and the result is the sum of the outputs for the two individual cases. The results are expressions for the sum and difference signals in terms of the hybrid parameters; characteristic admittance and line lengths.

The next step is to calculate the dependence of hybrid parameters on the mechanical factors of tolerance build-up and temperature effects. This is done by expressing the stripline admittance as a function of stripwidth, strip thickness, dielectric constant and ground plane spacing.

1

WIDE MODE ANTENNA
CONFIGURATION

ANTENNA
CONFIGURATION
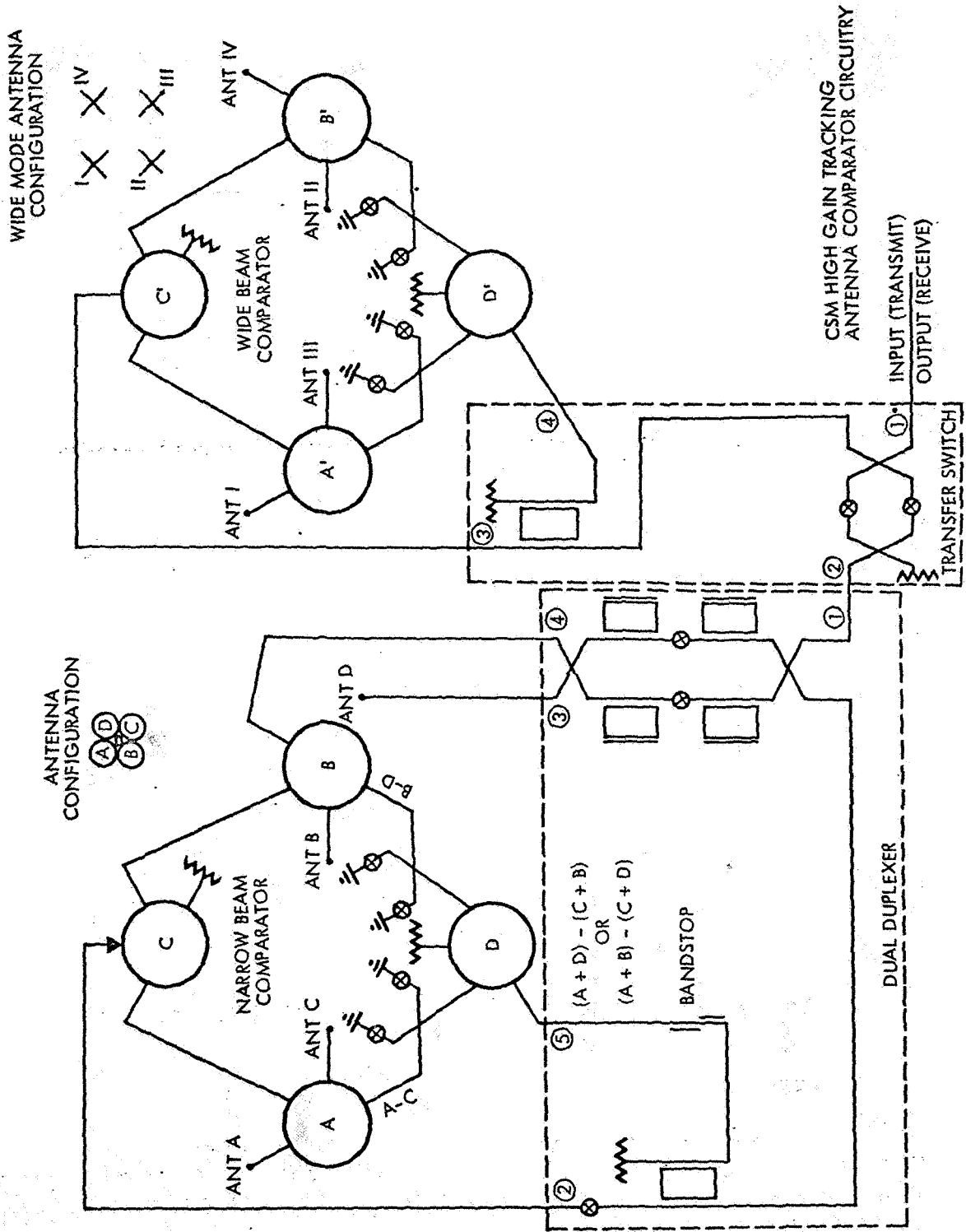
CSM HIGH GAIN TRACKING ANTENNA COMPARATOR CIRCUITRY

FIGURE 1

Finally, the stripline tolerances are evaluated and the worst-case combinations used to compute stripline parameters and thus hybrid performance for the worst-case values of hybrid parameters. The effect of temperature variation is also calculated by evaluating the effect of temperature on the stripline parameters and calculating the corresponding hybrid performance.

The 180° phase shifters in the comparators are used to change the sign of the difference signal so that it is either added to or subtracted from the sum signal. Time did not permit a detailed analysis of this part of the comparator so that the results presented for the errors contributed by the phase shifter are based on engineering estimates.

2.0 HYBRID ANALYSIS

2.1 INTRODUCTION

Basically, a hybrid junction is a four port network, as shown in
Figure 2 , constructed so that power incident at one port divides
equally into two of the other ports and does not pass directly to the
fourth, or conjugate port. Conversely, two equal inputs will produce
full output from one port and zero output from another, and two
arbitrary inputs at the appropriate ports will produce the vector sum
and difference at the other two ports. It is this latter property
which is utilized in a monopulse comparator.

The hybrid junctions used in the comparators for the CSM antenna
system are commonly known as $3\lambda/2$ hybrid rings because the network is
circular with a mean circumference of $3\lambda/2$, where λ is the wavelength
at the design frequency. To analyze this hybrid, use is made of the
method of Reed and Wheeler[1] which is based on the concept of even and
odd modes applied to symmetrical networks.

2.2 SYMMETRY ANALYSIS

A general four port symmetrical network is represented in Figure 3
showing the line of symmetry and the port numbering scheme. If two
signals of amplitude $\frac{1}{2}$ and in phase are applied to arms 1 and 4, because
of the symmetry no current flows across the line of symmetry. That is,
$I = 0$ and $Z = \infty$ and $Y = 0$ on the line of symmetry. This is the equiva-
lent of open circuits on the line of symmetry as shown in Figure 4 .
Similarly, if two signals of amplitude $\frac{1}{2}$ and out of phase are applied
to arms 1 and 4, a voltage null occurs at every point on the line of
symmetry. That is, $V = 0$ and $Z = 0$ and $Y = \infty$. This is the equiva-
lent of short circuits on the line of symmetry as shown in Figure 5 .
In each case, the problem reduces to that of a two arm network. For
the even mode, a reflection coefficient, Γ_{++}, and a transmission coeffi-
cient, T_{++}, are determined. For the odd mode, Γ_{+-} and T_{+-} are obtained.
The significance of Γ and T is shown in Figure 6 .
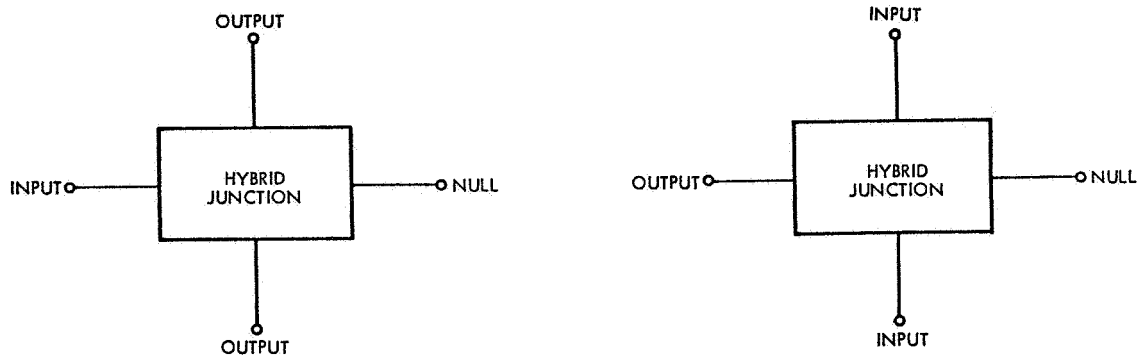
HYBRID JUNCTION BASIC PERFORMANCE

FIGURE 2
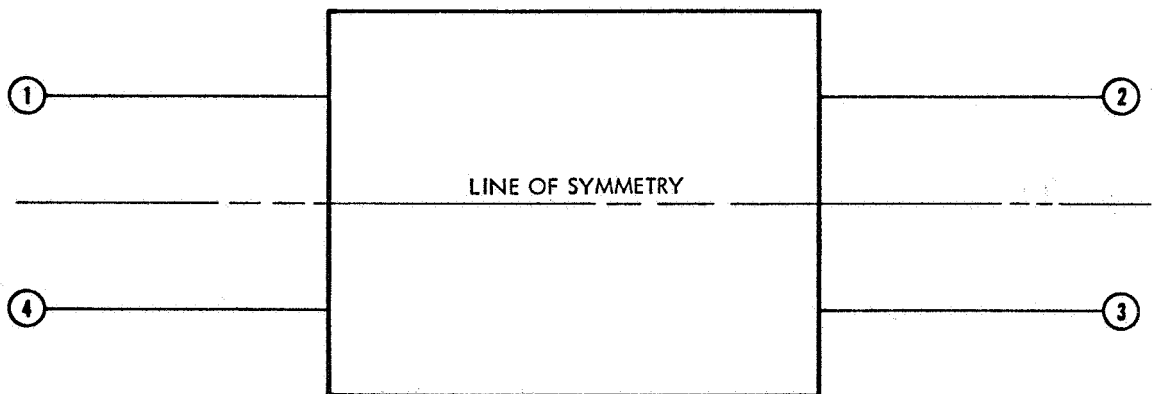
GENERAL FOUR PORT SYMMETRICAL NETWORK

FIGURE 3

5
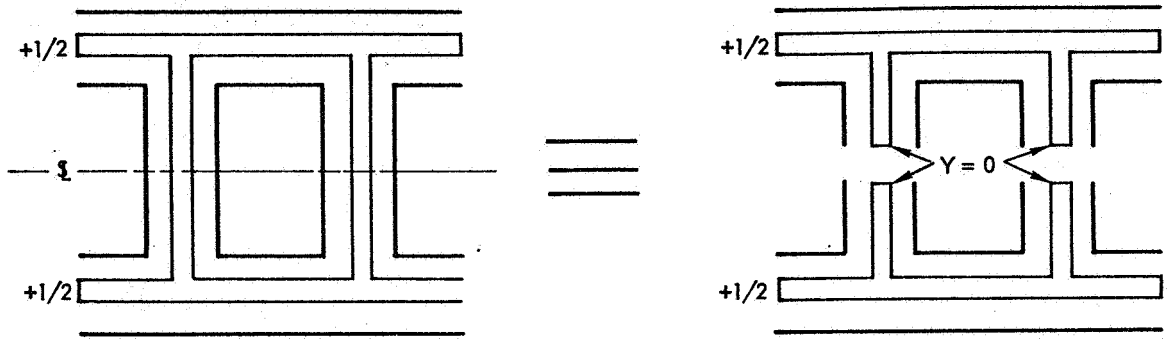
EVEN MODE REPRESENTATION OF SYMMETRICAL FOUR PORT

FIGURE 4
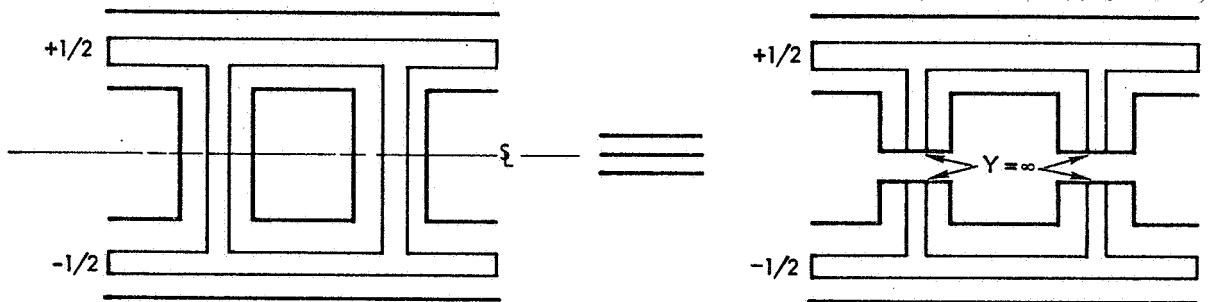
ODD MODE REPRESENTATION OF SYMMETRICAL FOUR PORT

FIGURE 5
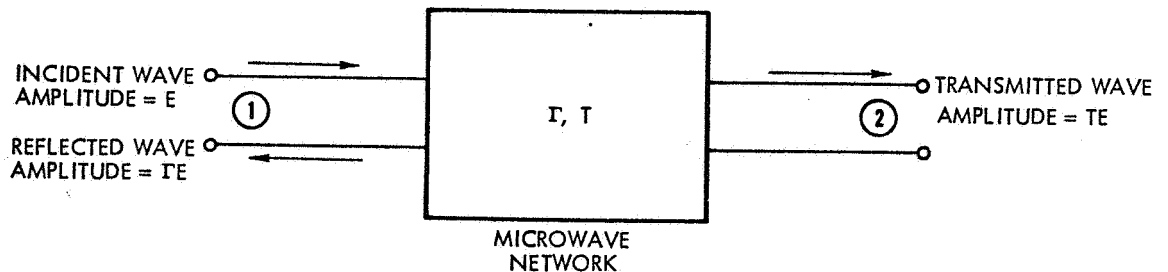
TWO PORT NETWORK CHARACTERIZED BY Γ AND T

FIGURE 6

6

By superposition, the sum of the even and odd mode cases is the case of a single signal of unit amplitude applied to arm 1 as shown in Figure 7 . The resultant signals out of the four arms are also the superposition of the signals obtained in the even mode case and in the odd mode case. Thus, letting A represent the emerging signal from each port, the vector amplitudes for the emerging signals for the sum of the even and odd mode cases above are:

$$
\begin{aligned}
A_1 &= \tfrac{1}{2}\,\Gamma_{++} + \tfrac{1}{2}\,\Gamma_{+-} \\
A_2 &= \tfrac{1}{2}\,T_{++} + \tfrac{1}{2}\,T_{+-} \\
A_3 &= \tfrac{1}{2}\,T_{++} - \tfrac{1}{2}\,T_{+-} \\
A_4 &= \tfrac{1}{2}\,\Gamma_{++} - \tfrac{1}{2}\,\Gamma_{+-}
\end{aligned}
\right\}
\tag{1}
$$

2.3 MATRIX ANALYSIS

The analysis of a cascade of two-terminal pair networks can be carried out by use of the ABCD matrix. The voltages and currents of a two port network can be related by several different sets of network parameters. The matrix equation relating the input voltage and current to the output voltage and current is shown in Figure 8a and defines the ABCD matrix. If several two port networks are cascaded, then the input quantities are related by the overall ABCD matrix which is the product of the individual network ABCD matrices as shown in Figure 8b . The ABCD matrices of some typical two port networks are shown in Figure 9 . It can be shown that the quantities Γ and T can be expressed in terms of the elements of the ABCD matrix as follows:

Voltage Reflection Coefficient $= \cdot$ $\Gamma = \dfrac{A+B-C-D}{A+B+C+D}$ (2)
With Matched Load

Voltage Transmission Coefficient $=$ $T = \dfrac{2}{A+B+C+D}$ (3)
With Matched Generator and Matched Load
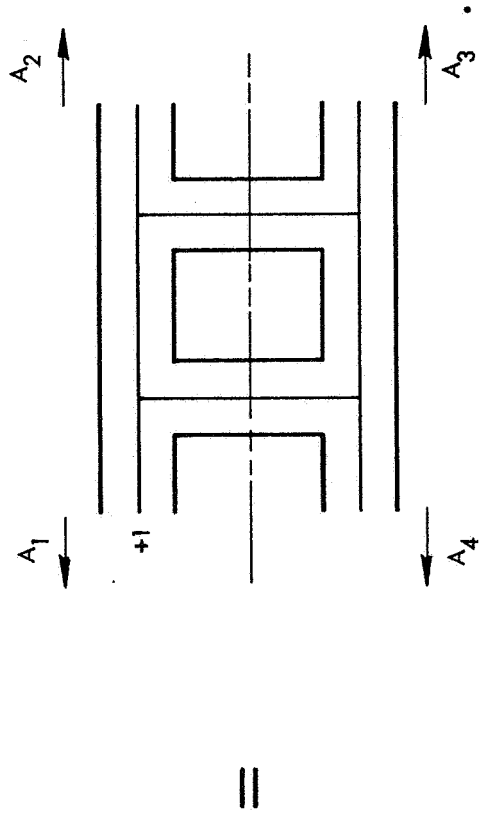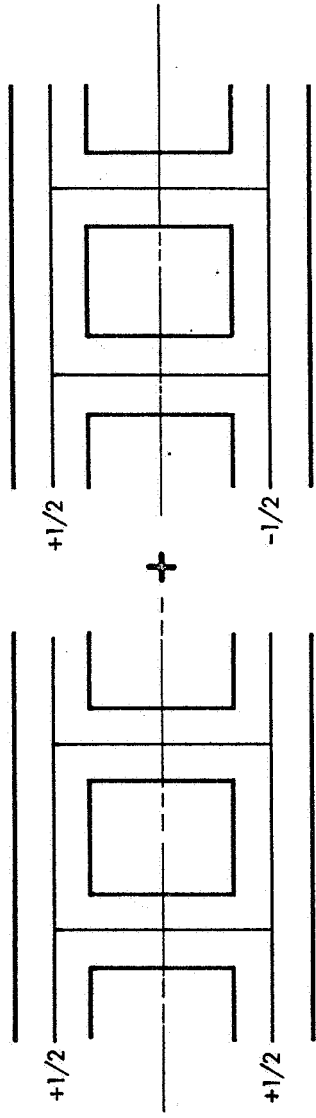
SUPERPOSITION OF EVEN AND ODD MODES

FIGURE 7

8

$$\begin{bmatrix} E_1 \\ I_1 \end{bmatrix} = \begin{bmatrix} A & B \\ C & D \end{bmatrix} \begin{bmatrix} E_2 \\ I_2 \end{bmatrix}$$
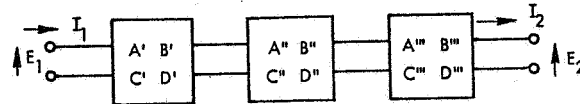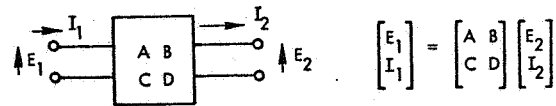
$$\begin{bmatrix} E_1 \\ I_1 \end{bmatrix} = \begin{bmatrix} A & B \\ C & D \end{bmatrix} \begin{bmatrix} E_2 \\ I_2 \end{bmatrix}$$

WHERE $\begin{bmatrix} A & B \\ C & D \end{bmatrix} = \begin{bmatrix} A' & B' \\ C' & D' \end{bmatrix} \begin{bmatrix} A'' & B'' \\ C'' & D'' \end{bmatrix} \begin{bmatrix} A''' & B''' \\ C''' & D''' \end{bmatrix}$

A) DEFINITION OF ABCD MATRIX
B) ABCD MATRIX OF CASCADED NETWORKS

FIGURE 8

SERIES IMPEDANCE, Z

$$M = \begin{bmatrix} 1 & Z \\ 0 & 1 \end{bmatrix}$$

SHUNT ADMITTANCE, Y

$$M = \begin{bmatrix} 1 & 0 \\ Y & 1 \end{bmatrix}$$

LENGTH OF LOSSLESS LINE:

CHARACTERISTIC IMPEDANCE, Zo
PROPAGATION CONSTANT, β
LENGTH, ℓ

$$M = \begin{bmatrix} \cos \beta\ell & jZ_o \sin \beta\ell \\ \dfrac{j}{Z_o} \sin \beta\ell & \cos \beta\ell \end{bmatrix}$$
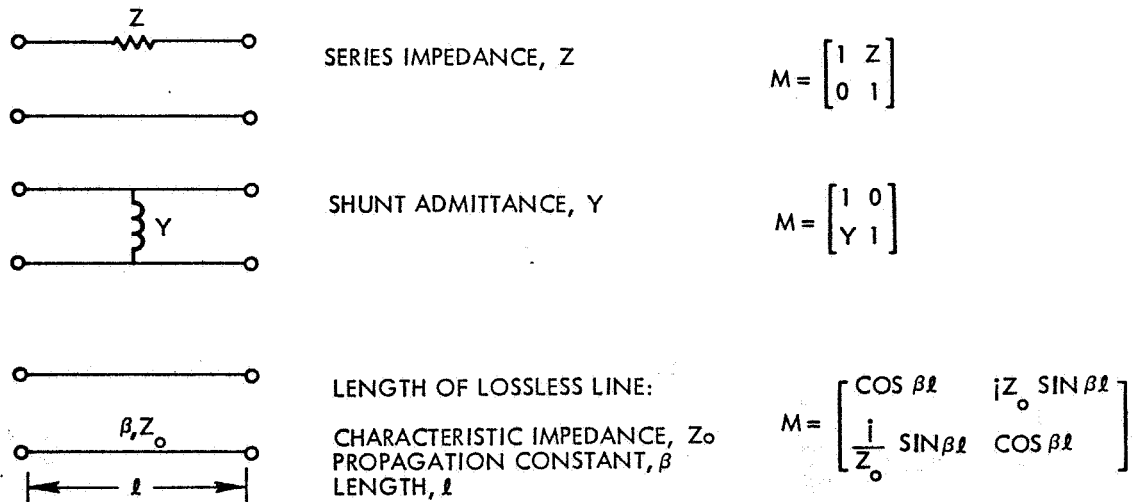
ABCD MATRICES OF TYPICAL TWO PORT NETWORKS

FIGURE 9

9

2.4 HYBRID ANALYSIS

2.4.1 Unit Signal Incident on Arm 1

The hybrid which is to be analyzed is shown in Figure 10. The circuit represents the stripline circuit which is used in the comparator circuit. In the usual hybrid, the ring admittance is constant and is equal to $Y_O/\sqrt{2}$ for a matched hybrid. However, in the narrow beam comparator, one of the hybrids is designed to give an unequal power split by variation of the ring admittance, so this variation must be accounted for in the analysis.

For the even mode when a unit signal is incident on arm 1, the hybrid can be represented as shown in Figure 11. The network then consists of a shunt stub $\lambda_O/8$ long with characteristic admittance Y_A, a line $\lambda_O/4$ long with characteristic admittance Y_B and a shunt stub $3\lambda_O/8$ long with characteristic admittance Y_A, all in cascade. λ_O is the wavelength at f_O, the design frequency. The electrical lengths of the lines are $\beta\ell$, where $\beta = \dfrac{2\pi}{\lambda}$ for stripline and λ is the wavelength at the frequency under consideration. Letting $\theta = \beta\ell$ for the $\lambda_O/8$ stub:

$$\theta = \frac{2\pi}{\lambda} \cdot \frac{\lambda_O}{8} = \frac{\lambda_O}{\lambda}\ \frac{\pi}{4}$$

The electrical length of the $\lambda_O/4$ line is 2θ and the electrical length of the $3\lambda_O/8$ stub is 3θ. For an open circuited line with characteristic admittance Y_O, the input admittance is given by $Y_{oc} = j\,Y_O \text{Tan}\,\beta\ell$.

For the $\lambda_O/8$ stub:

$$Y_{oc} = j\,Y_A \text{Tan}\,\theta$$

For the $3\lambda_O/8$ stub:

$$Y_{oc} = j\,Y_A \text{Tan}\,3\theta$$

The matrix for the first stub is therefore:
$$\begin{bmatrix} 1 & 0 \\ j\,Y_A \text{Tan}\,\theta & 1 \end{bmatrix},$$

LINE OF SYMMETRY

STRIPLINE HYBRID TO BE ANALYZED

$\frac{3\lambda_o}{4}$

Y_A

DIFFERENCE OUTPUT

Y_o

ANT NO. 2

Y_o

$\frac{\lambda_o}{4}$

Y_B

Y_B

$\frac{\lambda_o}{4}$

Y_A

ANT NO. 1

Y_o

$\frac{\lambda_o}{4}$

Y_o

SUM OUTPUT

λ_o = WAVELENGTH IN STRIPLINE AT DESIGN FREQUENCY, f_o
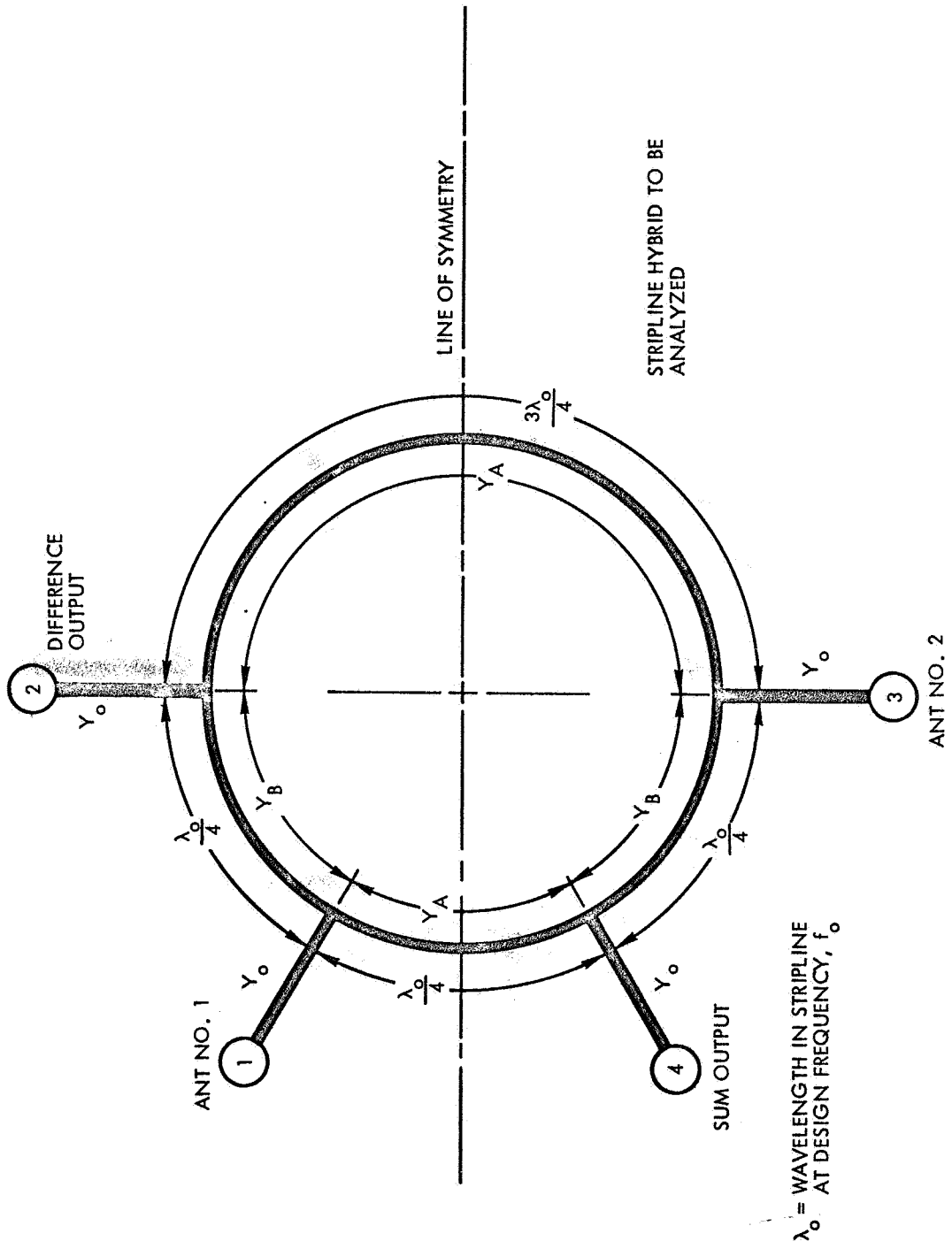
STRIPLINE HYBRID TO BE ANALYZED

FIGURE 10

11

and the matrix for the second stub is: $\begin{bmatrix} 1 & 0 \\ j\ Y_A \text{Tan } 3\theta & 1 \end{bmatrix}$,

and the matrix for the line between them is:

$$\begin{bmatrix} \text{Cos } 2\theta & \dfrac{j}{Y_B} \text{ Sin } 2\theta \\ j\ Y_B \text{Sin } 2\theta & \text{Cos } 2\theta \end{bmatrix}$$

The transmission matrix for the cascade network is the product of the individual transmission matrices taken in the order in which they occur. For the even mode network, as shown in Figure 11, the ABCD matrix, M_{++} , is given by:

$$M_{++} = \begin{bmatrix} 1 & 0 \\ j\ Y_A \text{Tan } \theta & 1 \end{bmatrix} \begin{bmatrix} \text{Cos } 2\theta & \dfrac{j}{Y_B} \text{ Sin } 2\theta \\ j\ Y_B \text{Sin } 2\theta & \text{Cos } 2\theta \end{bmatrix} \begin{bmatrix} 1 & 0 \\ j\ Y_A \text{Tan } 3\theta & 1 \end{bmatrix}$$

To simplify the algebra,

Let: $t = \text{Tan } \theta$

$$\text{Tan } 3\theta = \frac{3\ \text{Tan } \theta - \text{Tan}^3\theta}{1 - 3\ \text{Tan}^2\theta} = \frac{3t - t^3}{1 - 3t^2}$$

$$\text{Sin } 2\theta = \frac{2\ \text{Tan } \theta}{1 + \text{Tan}^2\theta} = \frac{2t}{1 + t^2}$$

$$\text{Cos } 2\theta = \frac{1 - \text{Tan}^2\theta}{1 + \text{Tan}^2\theta} = \frac{1 - t^2}{1 + t^2}$$

Then:

$$M_{++} = \begin{bmatrix} 1 & 0 \\ j\ Y_A\ t & 1 \end{bmatrix} \begin{bmatrix} \dfrac{1-t^2}{1+t^2} & \dfrac{j}{Y_B} \cdot \dfrac{2t}{1+t^2} \\ j\ Y_B \cdot \dfrac{2t}{1+t^2} & \dfrac{1-t^2}{1+t^2} \end{bmatrix} \begin{bmatrix} 1 & 0 \\ j\ Y_A \cdot \dfrac{3t-t^3}{1-3t^2} & 1 \end{bmatrix} \quad (4)$$

For the odd mode when a unit signal is incident on arm 1, the hybrid can be represented as shown in Figure 12. The network is the same as before except the stubs are shorted rather than opened. The input admittance of a shorted transmission line with characteristic admittance Y_0 is:
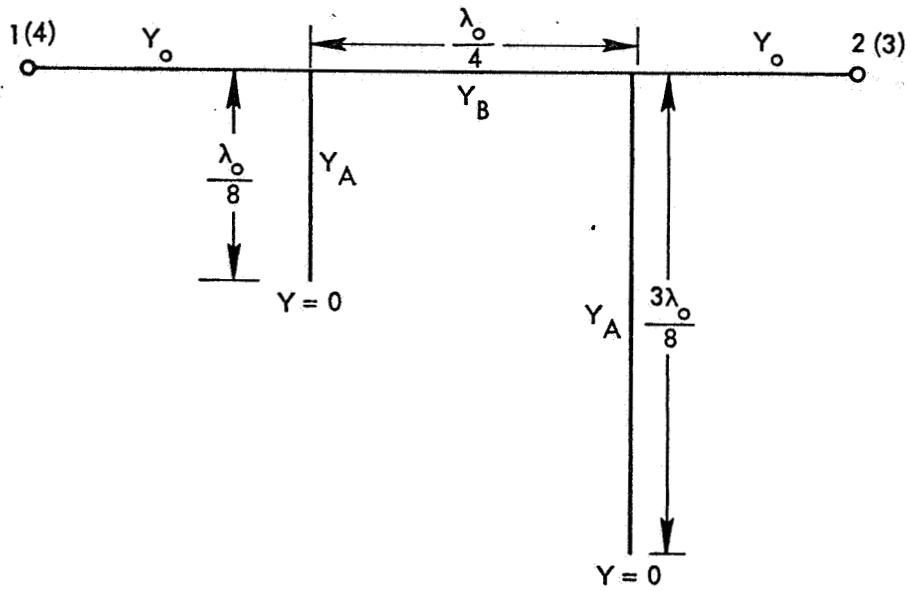
EVEN MODE REPRESENTATION, UNIT INPUT AT PORT 1

FIGURE 11
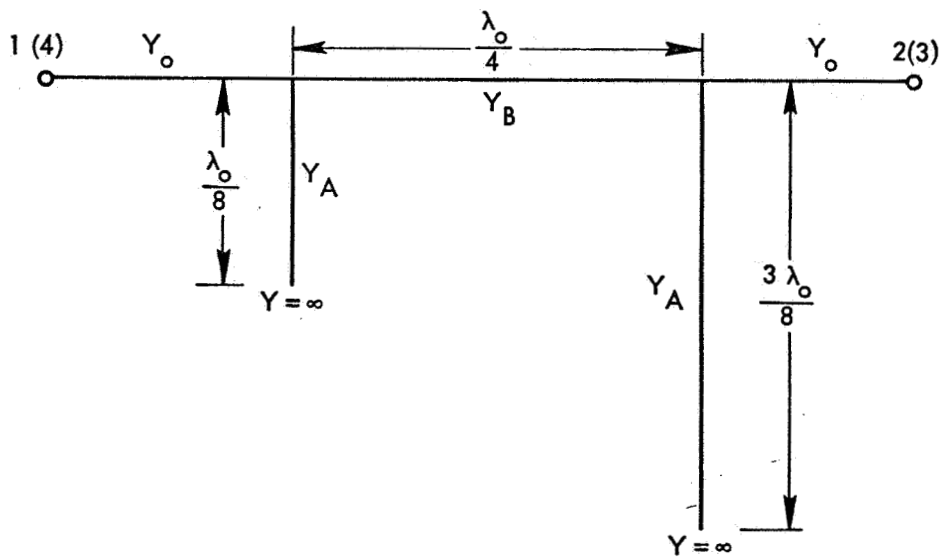
ODD MODE REPRESENTATION, UNIT INPUT AT PORT 1

FIGURE 12

13

$$Y_{SC} = -j\ Y_o \text{Cot}\ \beta\ell$$

For the $\lambda_o/8$ stub:

$$Y_{SC} = -j\ Y_A \text{Cot}\ \theta = -j\ Y_A/t$$

For the $3\lambda_o/8$ stub:

$$Y_{SC} = -j\ Y_A \text{Cot}\ 3\theta = -j\ Y_A \cdot \frac{1-3t^2}{3t-t^3}$$

For the odd mode network, as shown in Figure 12, the ABCD matrix, M_{+-} is given by:

$$M_{+-} = \begin{bmatrix} 1 & 0 \\ -j\ \dfrac{Y_A}{t} & 1 \end{bmatrix} \begin{bmatrix} \dfrac{1-t^2}{1+t^2} & \dfrac{j}{Y_B}\ \dfrac{2t}{1+t^2} \\ j\ Y_B \cdot \dfrac{2t}{1+t^2} & \dfrac{1-t^2}{1+t^2} \end{bmatrix} \begin{bmatrix} 1 & 0 \\ -j\ Y_A \cdot \dfrac{1-3t^2}{3t-t^3} & 1 \end{bmatrix} \quad (5)$$

Carrying out the matrix multiplication indicated in equations (4) and (5), following expressions are obtained for M_{++} and M_{+-}:

$$M_{++} = \begin{bmatrix} A_{++} & B_{++} \\ C_{++} & D_{++} \end{bmatrix} =$$

$$\frac{1}{Y_B(1+t^2)} \begin{bmatrix} Y_B(1-t^2)-2\ Y_A t^2\ \dfrac{(3-t^2)}{(1-3t^2)} & j\ 2t \\[4mm] j\ 2t \left[Y_B^2 - Y_A^2 t^2\ \dfrac{(3-t^2)}{(1-3t^2)} + 2\ Y_A Y_B\ \dfrac{(1-t^2)^2}{(1-3t^2)} \right] & Y_B(1-t^2)-2\ Y_A t^2 \end{bmatrix}$$

$$M_{+-} = \begin{bmatrix} A_{+-} & B_{+-} \\ C_{+-} & D_{+-} \end{bmatrix} =$$

$$\frac{1}{Y_B(1+t^2)} \begin{bmatrix} Y_B(1-t^2)+2 \, Y_A \, \dfrac{(1-3t^2)}{(3-t^2)} & j \, 2t \\[3em] \dfrac{j2}{t}\left[Y_B^2 t^2 - Y_A^2 \, \dfrac{(1-3t^2)}{(3-t^2)} - 2 \, Y_A Y_B \, \dfrac{(1-t^2)^2}{(3-t^2)}\right] & Y_B(1-t^2)+2 \, Y_A \end{bmatrix}$$

Substituting these values of A_{++}, B_{++}, C_{++}, D_{++}; A_{+-}, B_{+-}, C_{+-} and D_{+-} into equations (2) and (3), the following expressions are obtained for the reflection and transmission coefficients:

$$\Gamma_{++} = \frac{-2 \, Y_A t^2(1+t^2)+jt\left[(1-Y_B^2)(1-3t^2)+Y_A^2 t^2(3-t^2)-2 \, Y_A Y_B(1-t^2)^2\right]}{Y_B(1-t^2)(1-3t^2)-4Y_A t^2(1-t^2)+jt\left[(1+Y_B^2)(1-3t^2)-Y_A^2 t^2(3-t^2)+2Y_A Y_B(1-t^2)^2\right]}$$

$$T_{++} = \frac{Y_B(1+t^2)(1-3t^2)}{Y_B(1-t^2)(1-3t^2)-4Y_A t^2(1-t^2)+jt\left[(1+Y_B^2)(1-3t^2)-Y_A^2 t^2(3-t^2)+2Y_A Y_B(1-t^2)^2\right]}$$

$$\Gamma_{+-} = \frac{-2Y_A t^2(1+t^2)+jt\left[(1-Y_B^2)t^2(3-t^2)+Y_A^2(1-3t^2)+2Y_A Y_B(1-t^2)^2\right]}{Y_B t^2(1-t^2)(3-t^2)+4Y_A t^2(1-t^2)+jt\left[(1+Y_B^2)t^2(3-t^2)-Y_A^2(1-3t^2)-2Y_A Y_B(1-t^2)^2\right]}$$

$$T_{+-} = \frac{Y_B t^2(1+t^2)(3-t^2)}{Y_B t^2(1-t^2)(3-t^2)+4Y_A t^2(1-t^2)+jt\left[(1+Y_B^2)t^2(3-t^2)-Y_A^2(1-3t^2)-2Y_A Y_B(1-t^2)^2\right]}$$

These values can then be substituted into equations (1) and the performance of the hybrid for various values of the parameters determined.

2.4.2 Unit Signal Incident on Arm 3

When operated as a monopulse comparator, signals are applied to two arms of the hybrid and the output taken from the remaining two arms. Referring to Figure 10, it is seen that sum and difference signals are obtained when signals are applied to arms 1 and 3, the sum arm is 4 and

the difference arm is 2. The expressions for the performance of the hybrid with a unit signal applied to arm 1 have just been derived and it is now necessary to derive the expressions for the performance when a unit signal is applied to arm 3.

For the even mode when a unit signal is incident on arm 3, the hybrid can be represented as shown in Figure 13, and the hybrid can be represented as shown in Figure 14 for the odd mode in this case. Comparison of Figures 13 and 14 with Figures 11 and 12, respectively, shows that the networks are identical in each case except that the input and output ports have been reversed. To calculate the new ABCD matrices, the order of multiplication of the individual ABCD matrices is simply reversed giving the following results:

$$\bar{M}_{++} = \begin{bmatrix} 1 & 0 \\ \dfrac{j\ Y_A t(3-t^2)}{1-3t^2} & 1 \end{bmatrix} \begin{bmatrix} \dfrac{1-t^2}{1+t^2} & \dfrac{j}{Y_B}\cdot\dfrac{2t}{1+t^2} \\ j\ Y_B \cdot \dfrac{2t}{1+t^2} & \dfrac{1-t^2}{1+t^2} \end{bmatrix} \begin{bmatrix} 1 & 0 \\ j\ Y_A t & 1 \end{bmatrix} \quad (6)$$

$$\bar{M}_{+-} = \begin{bmatrix} 1 & 0 \\ -j\ \dfrac{Y_A}{t}\ \dfrac{(1-3t^2)}{3-t^2} & 1 \end{bmatrix} \begin{bmatrix} \dfrac{1-t^2}{1+t^2} & \dfrac{j}{Y_B}\cdot\dfrac{2t}{1+t^2} \\ j\ Y_B \cdot \dfrac{2t}{1+t^2} & \dfrac{1-t^2}{1+t^2} \end{bmatrix} \begin{bmatrix} 1 & 0 \\ -j\ \dfrac{Y_A}{t} & 1 \end{bmatrix} \quad (7)$$

Carrying out the matrix multiplication indicated in equation (6) and (7), the following expressions are obtained for $\bar{M}_{++}$ and $\bar{M}_{+-}$ *:

$$\bar{M}_{++} = \begin{bmatrix} \bar{A}_{++} & \bar{B}_{++} \\ \bar{C}_{++} & \bar{D}_{++} \end{bmatrix} =$$

$$\frac{1}{Y_B(1+t^2)} \begin{bmatrix} Y_B(1-t^2) - 2Y_A t^2 & j\ 2t \\ j\ 2t\left[Y_B^2 + 2Y_A Y_B \dfrac{(1-t^2)}{(1-3t^2)} - Y_A^2 \dfrac{t^2(3-t^2)}{(1-3t^2)}\right] & Y_B(1-t^2)-2Y_A t^2\dfrac{(3-t^2)}{(1-3t^2)} \end{bmatrix}$$

* Throughout this report, the unbarred quantities are for a unit input at Arm 1 and the barred quantities are for a unit input at Arm 3.
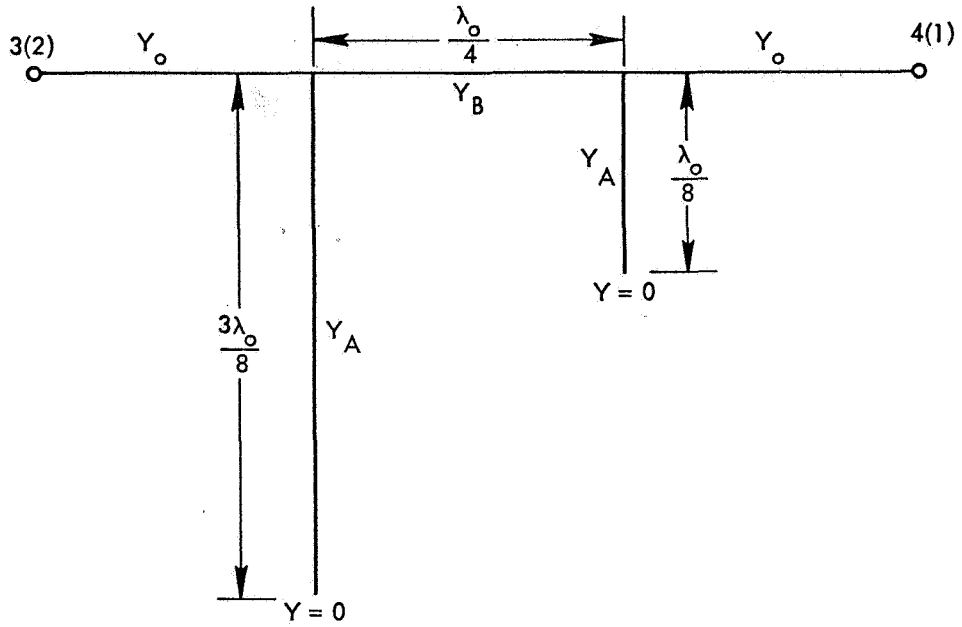
EVEN MODE REPRESENTATION, UNIT INPUT AT PORT 3

FIGURE 13
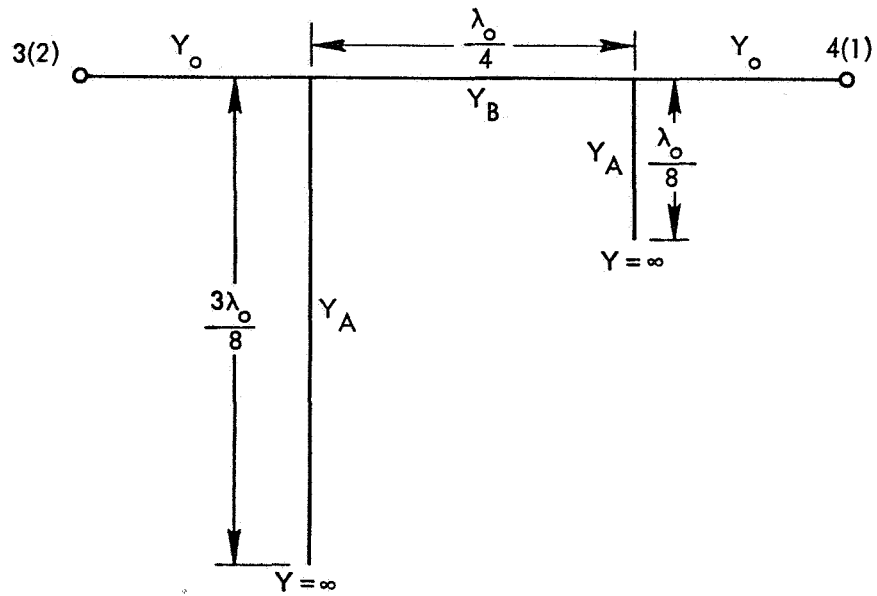
ODD MODE REPRESENTATION, UNIT INPUT AT PORT 3

FIGURE 14

17

$$\bar{M}_{+-} = \begin{bmatrix} \bar{A}_{+-} & \bar{B}_{+-} \\ \bar{C}_{+-} & \bar{D}_{+-} \end{bmatrix} =$$

$$\frac{1}{Y_B(1+t^2)} \begin{bmatrix} Y_B(1-t^2)+2Y_A & j\,2t \\[3mm] \dfrac{j2}{t}\left[Y_B^{\,2}t^2 - Y_A^{\,2}\dfrac{(1-3t^2)}{(3-t^2)} - 2Y_A Y_B \dfrac{(1-t^2)^2}{(3-t^2)} \right] & Y_B(1-t^2)+2Y_A\dfrac{(1-3t^2)}{(3-t^2)} \end{bmatrix}$$

Substituting these values of $\bar{A}_{++}$, $\bar{B}_{++}$, $\bar{C}_{++}$, $\bar{D}_{++}$; $\bar{A}_{+-}$, $\bar{B}_{+-}$, $\bar{C}_{+-}$ and $\bar{D}_{+-}$ into equations (2) and (3) the following expressions are obtained for the reflection and transmission coefficients:

$$\bar{\Gamma}_{++} = \frac{2Y_A t^2(1+t^2)+jt\left[(1-Y_B^{\,2})(1-3t^2)+Y_A^{\,2}t^2(3-t^2)-2Y_A Y_B(1-t^2)^2\right]}{Y_B(1-t^2)(1-3t^2)-4Y_A t^2(1-t^2)+jt\left[(1+Y_B^{\,2})(1-3t^2)-Y_A^{\,2}t^2(3-t^2)+2Y_A Y_B(1-t^2)^2\right]}$$

$$\bar{T}_{++} = \frac{Y_B(1+t^2)(1-3t^2)}{Y_B(1-t^2)(1-3t^2)-4Y_A t^2(1-t^2)+jt\left[(1+Y_B^{\,2})(1-3t^2)-Y_A^{\,2}t^2(3-t^2)+2Y_A Y_B(1-t^2)^2\right]}$$

$$\bar{\Gamma}_{+-} = \frac{2Y_A t^2(1+t^2)+jt\left[(1-Y_B^{\,2})t^2(3-t^2)+Y_A^{\,2}(1-3t^2)+2Y_A Y_B(1-t^2)^2\right]}{Y_B t^2(1-t^2)(3-t^2)+4Y_A t^2(1-t^2)+jt\left[(1+Y_B^{\,2})t^2(3-t^2)-Y_A^{\,2}(1-3t^2)-2Y_A Y_B(1-t^2)^2\right]}$$

$$\bar{T}_{+-} = \frac{Y_B t^2(1+t^2)(3-t^2)}{Y_B t^2(1-t^2)(3-t^2)+4Y_A t^2(1-t^2)+jt\left[(1+Y_B^{\,2})t^2(3-t^2)-Y_A^{\,2}(1-3t^2)-2Y_A Y_B(1-t^2)^2\right]}$$

As before, by superposition the vector amplitudes of the emerging signals from each arm for a unit signal applied to arm 3 can be found by summing the emerging signals for the even mode and the odd mode cases with the following results:

$$\bar{A}_3 = \frac{1}{2}\bar{\Gamma}_{++} + \frac{1}{2}\bar{\Gamma}_{+-}$$

$$\bar{A}_4 = \frac{1}{2}\bar{T}_{++} + \frac{1}{2}\bar{T}_{+-}$$

$$\bar{A}_1 = \frac{1}{2}\bar{T}_{++} - \frac{1}{2}\bar{T}_{+-}$$

$$\bar{A}_2 = \frac{1}{2}\bar{\Gamma}_{++} - \frac{1}{2}\bar{\Gamma}_{+-}$$

$$\left. \right\} \quad (8)$$

3.0 COMPARATOR ANALYSIS

3.1 SIGNAL OUTPUT ANALYSIS

In section 2.4, expressions for the vector outputs of hybrid ring with a signal applied to one terminal were derived for two separate input terminals. When the hybrid is used as a comparator, coherent signals are applied simultaneously to two ports, and their sum and difference are the outputs of the other ports. Again using the principle of super-position, the vector amplitude of the output at any port when multiple input terminals are excited simultaneously by coherent signals is the sum of the output signals calculated when each input port is excited separately.

Referring to Figure 10, when ports 1 and 3 are the antenna terminals, port 4 is the sum output and port 2 is the difference output. To write the expression for the outputs of ports 4 and 2 when unit amplitude, in phase signals are applied to arms 1 and 3 is simply a matter of adding the outputs for the separate cases. These are derived in section 2.4 and given in equations (1) and (8).

$$\text{SUM OUTPUT} = \Sigma = A_4 + \bar{A}_4 = \frac{1}{2} (\Gamma_{++} - \Gamma_{+-} + \bar{T}_{++} + \bar{T}_{+-}) \tag{9}$$

$$\text{DIFFERENCE OUTPUT} = \Delta = A_2 + \bar{A}_2 = \frac{1}{2} (T_{++} + T_{+-} + \bar{\Gamma}_{++} - \bar{\Gamma}_{+-}) \tag{10}$$

If the unit signal at port 3 has a phase angle of ψ with respect to the unit signal at port 1, equations (8) becomes:

$$\left.\begin{aligned}
\bar{A}_3 &= \frac{1}{2} (\bar{\Gamma}_{++} + \bar{\Gamma}_{+-}) \, e^{j\psi} \\
\bar{A}_4 &= \frac{1}{2} (\bar{T}_{++} + \bar{T}_{+-}) \, e^{j\psi} \\
\bar{A}_1 &= \frac{1}{2} (\bar{T}_{++} - \bar{T}_{+-}) \, e^{j\psi} \\
\bar{A}_2 &= \frac{1}{2} (\bar{\Gamma}_{++} - \bar{\Gamma}_{+-}) \, e^{j\psi}
\end{aligned}\right\} \tag{11}$$

and equations (9) and (10) become:

$$\Sigma = \frac{1}{2} \left(\Gamma_{++} - \Gamma_{+-} + \bar{T}_{++} e^{j\psi} + \bar{T}_{+-} e^{j\psi} \right) \tag{12}$$

$$\Delta = \frac{1}{2} \left(T_{++} + T_{+-} + \bar{\Gamma}_{++} e^{j\psi} - \bar{\Gamma}_{+-} e^{j\psi} \right) \tag{13}$$

Substituting the expressions for the Γ's and T's from section 2.4, the following expressions for Σ and Δ are obtained:

$$\Sigma = \frac{1}{2}\left[\frac{-2Y_A^2 t^2(1+t^2)+jt\left[(1-Y_B^2)(1-3t^2)+Y_A^2 t^2(3-t^2)-2Y_A Y_B(1-t^2)\right]}{Y_B(1-t^2)(1-3t^2)-4Y_A^2 t^2(1-t^2)+jt\left[(1+Y_B^2)(1-3t^2)-Y_A^2 t^2(3-t^2)+2Y_A Y_B(1-t^2)\right]} \right.$$

$$- \frac{-2Y_A^2 t^2(1+t^2)+jt\left[(1-Y_B^2)t^2(3-t^2)+Y_A^2(1-3t^2)+2Y_A Y_B(1-t^2)\right]}{Y_B t^2(1+t^2)(3-t^2)+4Y_A^2 t^2(1-t^2)+jt\left[(1+Y_B^2)t^2(3-t^2)-Y_A^2(1-3t^2)-2Y_A Y_B(1-t^2)\right]}$$

$$+ \frac{Y_B(1+t^2)(1-3t^2)}{Y_B(1-t^2)(1-3t^2)-4Y_A^2 t^2(1-t^2)+jt\left[(1+Y_B^2)(1-3t^2)-Y_A^2 t^2(3-t^2)+2Y_A Y_B(1-t^2)\right]}\, e^{j\psi}$$

$$\left. + \frac{Y_B t^2(1+t^2)(3-t^2)}{Y_B t^2(1-t^2)(3-t^2)+4Y_A^2 t^2(1-t^2)+jt\left[(1+Y_B^2)t^2(3-t^2)-Y_A^2(1-3t^2)-2Y_A Y_B(1-t^2)\right]}\, e^{j\psi} \right] \tag{14}$$

$$\Delta = \frac{1}{2}\left[\frac{Y_B(1+t^2)(1-3t^2)}{Y_B(1-t^2)(1-3t^2)-4Y_A^2 t^2(1-t^2)+jt\left[(1+Y_B^2)(1-3t^2)-Y_A^2 t^2(3-t^2)+2Y_A Y_B(1-t^2)\right]} \right.$$

$$+ \frac{Y_B t^2(1+t^2)(3-t^2)}{Y_B t^2(1-t^2)(3-t^2)+4Y_A^2 t^2(1-t^2)+jt\left[(1+Y_B^2)t^2(3-t^2)-Y_A^2(1-3t^2)-2Y_A Y_B(1-t^2)\right]}\, e^{j\psi}$$

$$+ \frac{-2Y_A^2 t^2(1+t^2)+jt\left[(1-Y_B^2)(1-3t^2)+Y_A^2 t^2(3-t^2)-2Y_A Y_B(1-t^2)\right]}{Y_B(1-t^2)(1-3t^2)-4Y_A^2 t^2(1-t^2)+jt\left[(1+Y_B^2)(1-3t^2)-Y_A^2 t^2(3-t^2)+2Y_A Y_B(1-t^2)\right]}\, e^{j\psi}$$

$$\left. - \frac{2Y_A^2 t^2(1+t^2)+jt\left[(1-Y_B^2)t^2(3-t^2)+Y_A^2(1-3t^2)+2Y_A Y_B(1-t^2)\right]}{Y_B t^2(1-t^2)(3-t^2)+4Y_A^2 t^2(1-t^2)+jt\left[(1+Y_B^2)t^2(3-t^2)-Y_A^2(1-3t^2)-2Y_A Y_B(1-t^2)\right]}\, e^{j\psi} \right] \tag{15}$$

22

The expression for the sum and difference outputs can be programmed for computation on a digital computer and the performance for various combinations of values of Y_A, Y_B, and t can be determined. For the ideal hybrid, $Y_A = Y_B = 1/\sqrt{2}$, t = 1 at the design frequency and the expressions for Σ and Δ become:

$$\Sigma = (-j\sqrt{2} \, \cos \tfrac{\psi}{2})e^{j\frac{\psi}{2}} \tag{16}$$

$$\Delta = (-\sqrt{2} \, \sin \tfrac{\psi}{2})e^{j\frac{\psi}{2}} \tag{17}$$

When $\psi = 0$, $\Sigma = -j\sqrt{2}$ and $\Delta = 0$.

3.2 STRIPLINE ADMITTANCE ANALYSIS

According to Cohn[2] the characteristic impedance of a stripline is given by:

$$Z_o = \frac{94.15/\sqrt{\epsilon_r}}{\left[\dfrac{W/b}{1-t/b} + \dfrac{C'f}{0.0885\epsilon_r}\right]}$$

Where:

$$C'f = \frac{0.0885}{\pi}\epsilon_r\left\{\frac{2}{1-t/b}\ell n\left[\frac{1}{1-t/b}+1\right]-\left(\frac{1}{1-t/b}-1\right)\ell n\left[\frac{1}{(1-t/b)^2}-1\right]\right\}\mu\mu f/cm$$

ϵ_r is the relative dielectric constant of the medium and W, t and b are defined in Figure 15. The computer was programmed to compute the characteristic impedance and the normalized admittance of stripline using the above equations.
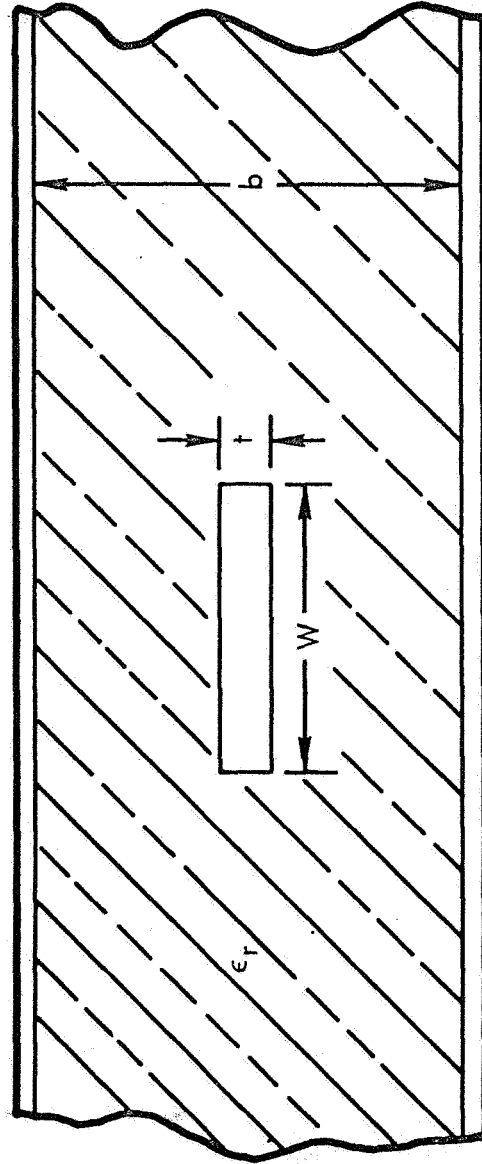
STRIPLINE CROSS SECTION

FIGURE 15

3.3 DIMENSIONAL ANALYSIS

The next step in the analysis is to calculate from the drawings of the comparator the amount of variation in stripline dimensions, which cause the admittances and the lengths of lines of the various parts of the hybrid ring to change. The worst case combinations can then be selected and the stripline parameters computed which lead to the extreme values of comparator performance. Ordinarily, the dimensions and their tolerances would be taken directly from the drawing, but in the case of the narrow beam and wide beam comparators, the only stripline drawings available were copies of the artwork. These drawings had a scale line and a few irrelevant dimensions. The artwork drawings for the two comparators were measured and remeasured to establish reasonable dimensions for the hybrid rings. Using the scale line to reduce the measurements, the mean diameters of the hybrids and the strip width of 50 Ω feed line measured very close to the theoretical values for the ideal hybrid, but the stripwidths of the rings did not. An alternative scale factor giving the correct ring stripwidth and incorrect ring diameters and feed line stripwidths was also tried. The percentage error in the latter case was larger than in the former, so the scale factor giving the correct ring diameters was used. The dual diplexer and transfer switch drawings, however, did have complete dimensions and tolerances for the stripline circuitry. The tolerances given for these drawings were assumed to apply to the artwork for both comparators, and the tolerances assumed are shown in Figure 16.

All hybrids consist of a single trace of one ounce copper between two 1/8 inch sheets of irradiated polyolefin plus a 0.020" thick spacer of irradiated polyolefin. The thickness of one ounce copper is $0.0014" \pm 10\% = \frac{0.00156"}{0.00126"}$. The dielectric constant of irradiated polyolefin is given by the manufacturer as 2.32 ± 0.01. The ground plane spacing is $0.271" \pm 0.005"$ according to North American Aviation[3].

The scaled dimensions of the various hybrids of the narrow beam comparator are shown in Figures 17, 18 and 19. Hybrid A is the hybrid

R₁ ±0.004 IN.

R₂ ± 0.004 IN.

W ± 0.004 IN
FOUR PLACES

60° ±1/4°
THREE PLACES
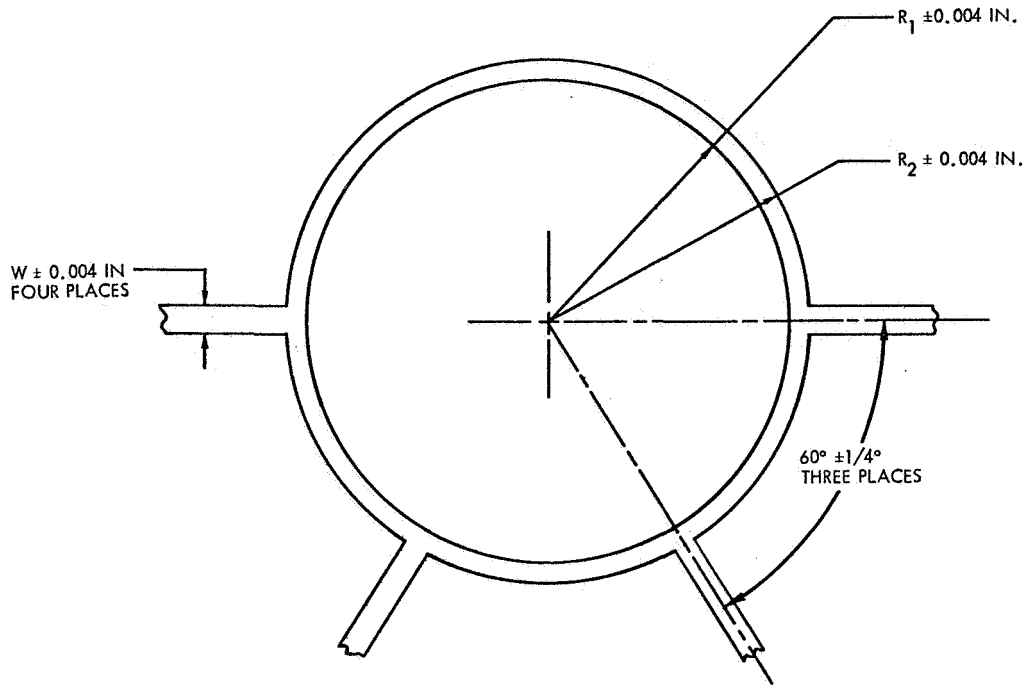
HYBRID TOLERANCES

FIGURE 16

R₁

R₂

R₃

R₄

W₂ (TWO PLACES)

W₁ (FOUR PLACES)

W₃ (TWO PLACES)
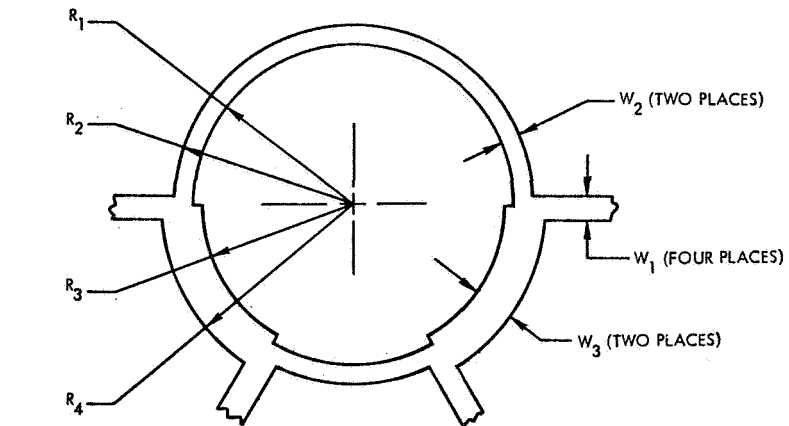
SCALED DIMENSIONS

R_1 = 0.8225 IN.

R_2 = 0.9375 IN.

R_3 = 0.8135 IN.

R_4 = 0.9465 IN.

W_1 = 0.224 IN.

W_2 = 0.115 IN.

W_3 = 0.133 IN.

MEAN DIAMETER = 1.760 IN.
f_o = 2106 MHz

NARROW BEAM HYBRID A DIMENSIONS

FIGURE 17

SCALED DIMENSIONS

R_1 = 0.815 IN.

R_2 = 0.945 IN.

W_1 = 0.224 IN.

W_2 = 0.130 IN.

MEAN DIAMETER = 1.760 IN.

f_o = 2106 MHz
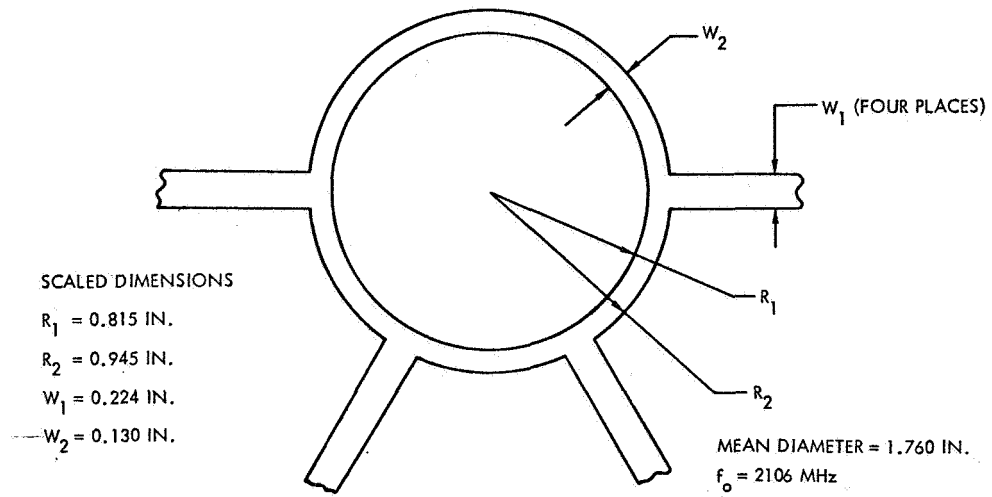
NARROW BEAM HYBRIDS B AND D DIMENSIONS

FIGURE 18

SCALED DIMENSIONS

R_1 = 0.779 IN.

R_2 = 0.909 IN.

W_1 = 0.224 IN.

W_2 = 0.130 IN.

MEAN DIAMETER = 1.688 IN.

f_o = 2193 MHz
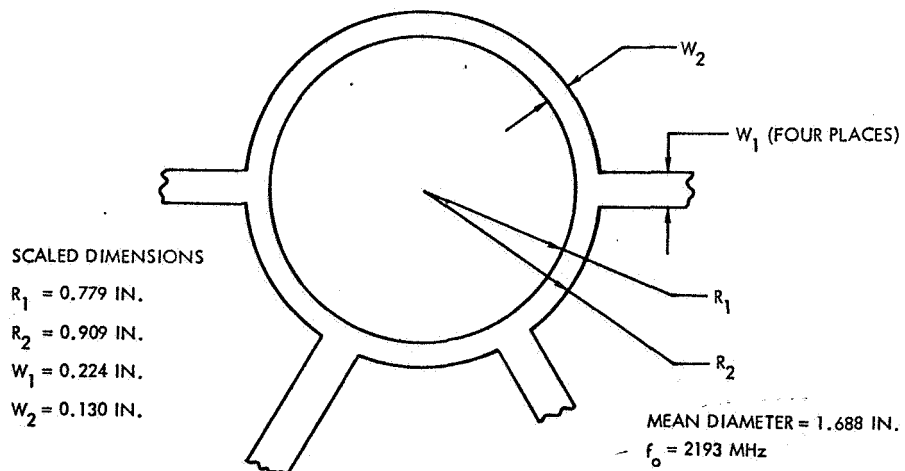
NARROW BEAM HYBRID C DIMENSIONS

FIGURE 19

27

which sums antennas A and C, Hybrid B is the hybrid which sums antennas B and D, Hybrid C is the hybrid which sums the sum outputs of Hybrids A and B, and Hybrid D is the hybrid which sums the difference outputs of Hybrids A and B as shown in Figure 1 . Hybrid A has unequal ring widths because it is designed for an unequal power split to compensate for additional attenuation in the antenna D feed path due to its extra length.

Using the tolerances in Figure 16 and the dimensions in Figures 17, 18 and 19, the following tables of extreme dimensions can be made:

HYBRID A $W_1 = 0.224"$ $\pm 0.004"$

$R_1(in)$	$R_2(in)$	$W_2(in)$	$R_3(in)$	$R_4(in)$	$W_3(in)$	$f_o(MHz)$
0.8225	0.9375	0.115	0.8135	0.9465	0.133	2106
0.8265	0.9335	0.107	0.8175	0.9425	0.125	2106
0.8185	0.9415	0.123	0.8095	0.9505	0.141	2106

HYBRID B & D $W_1 = 0.224"$ $\pm 0.004"$

$R_1(in)$	$R_2(in)$	$W_2(in)$	$f_o(MHz)$
0.815	0.945	0.130	2106
0.811	0.949	0.138	2106
0.819	0.941	0.122	2106

HYBRID C $W_1 = 0.224"$ $\pm 0.004"$

$R_1(in)$	$R_2(in)$	$W_2(in)$	$f_o(MHz)$
0.779	0.909	0.130	2193
0.775	0.913	0.138	2193
0.783	0.905	0.122	2193

The extreme values of ring width for Hybrids B, C and D are: $W_2 = \frac{0.138"}{0.122"}$. The extreme values of ring widths for Hybrid A are:

$$W_2 = \frac{0.123"}{0.107"} \quad \text{and} \quad W_3 = \frac{0.141"}{0.125"} \quad .$$

The center frequency of the hybrids at the dimensional extremes is always the same as the design frequency, so that the worst case effects of width variation on comparator performance can be computed at the design frequency.

3.4 ADMITTANCE VARIATION ANALYSIS

The characteristic admittance of a stripline is proportional to the capacity between the center conductor and the ground planes. The stripline capacity increases as:

- Stripwidth is increased.
- Strip thickness is increased.
- Dielectric constant is increased.
- Ground plane spacing is decreased.

For any particular trace (strip) Y_{max} occurs for W_{max}, t_{max}, ϵ_{max} and b_{min}; likewise, Y_{min} occurs for W_{min}, t_{min}, ϵ_{min} and b_{max}. For a particular comparator package, all parameters should be very nearly the same throughout the whole package <u>except</u> for W, the strip width. For any package, then, the extreme values of admittance for a particular strip width would be obtained when the other parameters were all at the maximum or minimum capacity conditions. For the narrow and wide beam comparators, these conditions are:

For Y_{max} : $b = 0.266''$
(Maximum Capacity) $t = 0.00154''$
                       $\epsilon_r = 2.33$

For Y_{min} : $b = 0.276''$
(Minimum Capacity) $t = 0.00126''$
                       $\epsilon_r = 2.31$

Using the computer program, we can calculate the values of Y for the extreme values of W for the maximum and minimum admittance conditions. The results are shown in the following tables:

MAXIMUM CAPACITY CONDITION			
b = .266"	t = 0.00154"	ε$_r$ = 2.33	
W(Ring)"	Y(Normalized)	W(Arm)"	Y(Normalized)
0.122	0.7419522	0.220	1.0423479
0.138	0.79099639	0.228	1.06687
0.107	0.69597326		
0.123	0.74501746		
0.125	0.75114798		
0.141	0.80019218		

MINIMUM CAPACITY CONDITION			
b = .276"	t = 0.00126"	ε$_r$ = 2.31	
W(Ring)"	Y(Normalized)	W(Arm)"	Y(Normalized)
0.122	0.72293551	0.220	1.0108475
0.138	0.76994156	0.228	1.0343505
0.107	0.67886733		
0.123	0.72587338		
0.125	0.73174914		
0.141	0.77875519		

Referring to Figures 17, 18 and 19, let the normalized admittances associated with stripline widths W_1, W_2 and W_3 be called Y_1, Y_2 and Y_3 respectively. The largest errors in hybrid performance will occur when the ratios of ring admittance to arm admittance, Y_2/Y_1 and Y_3/Y_1, are furthest from $1/\sqrt{2}$. To find the extreme values various admittance ratios were calculated for the hybrids for both the maximum and minimum capacity cases, and the results are presented in the following tables:

HYBRID A

	Admittance or Admittance Ratio	
	Maximum Capacity	Minimum Capacity
Max Y_2	0.74501746	0.72587338
Min Y_2	0.69597326	0.67886733
Max Y_3	0.80019218	0.77875519
Min Y_3	0.75114798	0.73174914
Max Y_1	1.06687	1.0343505
Min Y_1	1.0423479	1.0108475
Max Y_2/Min Y_1	0.71474933	0.71808396
Max Y_3/Min Y_1	0.76768244	0.77039829
Min Y_2/Max Y_1	0.65235058	0.65632233
Min Y_3/Max Y_1	0.70406702	0.70744795
Min Y_2/Min Y_1	0.66769767	0.67158234
Min Y_3/Min Y_1	0.72063078	0.72389667
Max Y_2/Max Y_1	0.69832075	0.70176732
Max Y_3/Max Y_1	0.75003719	0.75289294

HYBRIDS B, C AND D

	Admittance or Admittance Ratio	
	Maximum Capacity	Minimum Capacity
Max Y_2	0.79099639	0.76994156
Min Y_2	0.7419522	0.72293551
Max Y_1	1.06687	1.0343505
Min Y_1	1.0423479	1.0108475
Max Y_2/Min Y_1	0.75886025	0.76167924
Min Y_2/Max Y_1	0.69544716	0.69892701

From these values of admittance ratios, the worst case values can be selected and used to compute the hybrid performance.

3.5 MECHANICAL ANGLE TOLERANCE ANALYSIS

The analysis of the hybrid based on symmetry considerations does not allow the inclusion of the effect of angular errors between the various ports. The error in hybrid performance due to angular tolerance build-up is calculated as follows. Referring to Figure 10, if both the angle between arms 1 and 2 and the angle between 1 and 4 are at the upper limit, that portion of the hybrid looks longer electrically, and the remaining portion looks shorter electrically. Conversely, if the above angles are both at the lower limit, the paths between arms 1 and 2 and between arms 1 and 4 looks shorter electrically while the remaining portion looks electrically longer. In either of the above cases, the effect on the sum and difference output can be considered to be the same as if the operating frequency were changed up or down by an amount corresponding to the apparent change in size of the hybrid. The amount of error introduced by the angle error is then computed by calculating the hybrid performance at frequencies above and below the design frequency by an amount corresponding to the change in phase shift introduced by the worst case angle tolerance build-up. 60 ± 0.25 mechanical degrees as shown in Figure 16, correspond to 90 ± 0.375 electrical degrees. A change in phase shift of $\frac{\pm 0.375°}{90°}$ corresponds to a change in operating frequency of ± 0.416 percent, so the hybrid performance is calculated over a 0.8333 percent bandwidth to account for angle tolerance build-up. This analysis is not as rigorous as that for the other tolerances, but since the variations are small, it is believed that the errors so computed will be within one or two percent of the true value.

The other situation in which one angle is at the upper limit and the other is at the lower limit will tend to be self-compensating for the small angles involved and the effect on the magnitudes should be negligible.

3.6 TEMPERATURE EFFECT ANALYSIS

3.6.1 Hybrid Ring Performance

The analysis of the variation of comparator performance due to changing temperature is based on the following assumptions:

- The temperature variation of the stripline packages is from -85°F to $+120^\circ$F.

- There is no provision to compensate for temperature variation in the design or testing of the comparators.

- The dimensions of the stripline artwork are nominal at $+75^\circ$F.

- The stripline expansion and contraction due to temperature variation is determined principally by the thermal coefficient of expansion of irradiated polyolefin which is given by the manufacturer as 6×10^{-5} per $^\circ$F.

- The effects of thickness variations due to temperature change are negligible compared to those of the transverse dimensional changes caused by the same temperature variation.

The temperature variation from nominal, 75°F, is $+45^\circ$F and -160°F. The design frequency of hybrids A, B and D is 2106 MHz which requires a mean hybrid diameter of 1.760" at 75°F. The mean diameter of the hybrids will vary with temperature as follows:

$$D_1 = D_o + D_o K\Delta T$$

D_1 = new mean diameter

D_o = mean diameter at 75°F

K = thermal coefficient of expansion of irradiated polyolefin = $6 \times 10^{-5}/^\circ$F

ΔT = change in temperature

33

For the high temperature extreme:

$$D^+ = 1.760 + 1.760 \times 6 \times 10^{-5} \times 45$$
$$= 1.760 + .00475$$
$$D^+ = 1.7648" \ @ \ 120°F$$

For the low temperature extreme:

$$D^- = 1.760 + 1.760 \times 6 \times 10^{-5} \times (-160)$$
$$= 1.760 - .0169$$
$$D^- = 1.7431" \ @ \ -85°F$$

The corresponding values of center frequencies, f_o at the temperature extremes are:

$$f_o^+ = 2106 \times \frac{1.760}{1.7648} = 2100.27 \text{ MHz at } 120°F$$

$$f_o^- = 2106 \times \frac{1.760}{1.7341} = 2126.42 \text{ MHz at } -85°F$$

The design frequency of Hybrid C is 2193 MHz with a mean hybrid diameter of 1.688" at 75°F, and the center frequencies at the temperature extremes are calculated as above:

$$f_o^+ = 2187.04 \text{ MHz at } 120°F$$

$$f_o^- = 2214.25 \text{ MHz at } -85°F$$

To calculate the effects of temperature environment of the hybrids, the above values of f_o^+ and f_o^- are used in the computer program as the center frequency, and the performance is calculated at 2106 MHz.

3.6.2 Feed Line Differential Phase Shift

Unequal phase shift in the feed lines between the parabolic reflectors and the narrow beam comparators will shift the apparent position of the null and thus cause a boresight error. The feed lines for the narrow beam array are rigid aluminum coax and are approximately 62 inches long (they are trimmed to equal phase length in the assembly process). The temperature coefficient of expansion of aluminum is $28.7 \times 10^{-6}/^{\circ}C$. Assuming a maximum temperature differential of $60^{\circ}C$ ($90^{\circ}C$ to $150^{\circ}C$), the differential phase shift is calculated as follows:

$$\Delta\ell = \ell \times K \times \Delta t$$
$$= 62" \times 28.7 \times 10^{-6} \times 60 \qquad .$$
$$\Delta\ell = 0.107"$$

$$\Delta\varphi = \frac{\Delta\ell}{\lambda_{2106}} \times 360^{\circ} = \frac{0.107}{5.61} \times 360$$

$$\Delta\varphi = 6.85^{\circ}$$

The maximum phase error between any two lines of the narrow beam array due to temperature difference is therefore 6.85°.

For the wide beam array, the feed lines consist of approximately 10.5 inches of aluminum jacketed semi-rigid coax and 28 inches of flexible coax, both using irradiated polyolefin as their dielectric. Assuming that the change of length of the flexible cable will be controlled by the copper center conductor ($K = 0.9 \times 10^{-5}/^{\circ}F$), and the change of length of the semi-rigid coax will be controlled by the aluminum outer conductor ($K = 1.59 \times 10^{-5}/^{\circ}F$), the total change in length is calculated as follows:

$$\Delta\ell = \ell'K'\Delta t + \ell''K''\Delta t = (\ell'K' + \ell''K'')\Delta t$$
$$\Delta\ell = (10.5" \times 1.59 \times 10^{-5} + 28" \times 0.9 \times 10^{-5})\Delta t$$
$$\Delta\ell = 4.19 \times 10^{-4} \Delta t \text{ inches}$$

The proximity of all four wide beam feed lines over nearly all
their length eliminates the possibility of any but extremely small
temperature differences between the lines. Assuming a temperature
differential of $10^{\circ}F$ as a very conservative value, the differential
phase shift is calculated as:

$$\Delta\ell = 4.19 \times 10^{-4} \times 10"$$

$$\Delta\ell = 0.00419"$$

$$\Delta\varphi = \frac{\Delta\ell}{\lambda_{2106}/\sqrt{\epsilon_r}} \times 360^{\circ} = \frac{0.00419}{5.61} \times 1.532 \times 360$$

$$\Delta\varphi = 0.411^{\circ}$$

The maximum phase shift between any two lines of the wide beam array
due to temperature difference is therefore 0.411°.

3.7 DIODE PHASE SHIFTER PERFORMANCE (ESTIMATED)

There are two diode phase shifters in each comparator circuit as
shown in Figure 1. Each phase shifter consists of a 3 db directional
coupler and two pin diode assemblies. The purpose of these 180° phase
shifters is to periodically change the sign of the total difference
signal so that it is either added to or subtracted from the sum signal.
Because of insufficient time, a rigorous analysis of the phase shifter
was not performed but some estimates for errors introduced by the phase
shifter can be made.

3.7.1 Temperature Effects

The coupling factor of the stripline directional coupler was
calculated for changes in dimensions caused by temperature variation and
was found not to vary (in eight significant figures). A diode manu-
facturer and user indicates that the reflection coefficient of a pin
diode which is either full back-biased or forward-biased is not a function
of the temperature of the diode. It is therefore estimated that the
effect of temperature variation on the phase shifters is negligible.

36

3.7.2 Tolerance Buildup Effects

If the coupling of the directional coupler is not exactly 3 db, the result will be an increase in insertion loss due to reflection of some of the input power. The coupling factor of the directional coupler was calculated for the dimensional extremes. The worst coupling factor of -2.635db causes an additional insertion loss of 0.035db, so that the maximum amplitude unbalance into Hybrid D due to directional coupler manufacturing is 0.035db. The diode assemblies are adjusted in final assembly so that the resultant phase shift in each phase shifter is $180^{\circ} \pm 7^{\circ}$. This means that a maximum phase difference of 14° between the input signals to Hybrid D could be obtained. The pin diode assemblies have a requirement that their VSWR be at least 20:1 in the forward biased condition. This means that the insertion loss of the effective short caused by the diode must be less than 0.86db. It is estimated that the variation of insertion loss between diode switch assemblies due to differences in diodes will not exceed 0.15db. Therefore, the estimated maximum amplitude unbalance at the input of Hybrid D is 0.185db and the maximum phase difference is 14°.

4.0   CONCLUSIONS AND RESULTS

The previous sections have presented an analysis of the CSM-HGA microwave comparator circuit to determine the magnitude of the amplitude and phase errors caused by assembly tolerance buildups and by temperature variations. Expressions for the sum and difference outputs have been developed for a typical four port ring hybrid of the type used in the HGA microwave network. Since the expressions were too complex for hand computations, a computer program was developed for use in evaluating the model. Various CSM-HGA drawing data was consulted to determine the maximum and minimum circuit variations as a function of dimensional tolerances. These quantities will be incorporated into the CSM-HGA RF math model and will be instrumental in determining the final transfer function envelope or scale factor for the RF circuit. It was found that the pin diode switches produce negligible phase shift due to temperature variations and therefore the final transfer function will not be adversely affected by their operation.

The following sections present the pertinent results of the analysis.

4.1   FORM OF COMPUTER OUTPUT

Equations 12 and 13 give the sum and difference output voltages when unit voltages are incident on the antenna ports. These voltages are expressed in terms of reflection and transmission coefficients which are in turn functions of the hybrid parameters. To be used in the general mathematical model of the CSM High Gain Tracking Antenna System, it is desirable that the output voltages be expressed as a function of $1 + K\, e^{j\delta} e^{j\psi}$, where K represents the amplitude unbalance due to the hybrid and δ the phase unbalance introduced by the hybrid.[4] Dividing equation 12 by $(\Gamma_{++} - \Gamma_{+-})$ and equation 13 by $(T_{++} + T_{+-})$ results in the following expressions:

$$\frac{\Sigma}{(\Gamma_{++} - \Gamma_{+-})} = \frac{1}{2} \left[1 + \frac{(\bar{T}_{++} + \bar{T}_{+-})}{(\bar{\Gamma}_{++} - \bar{\Gamma}_{+-})} e^{j\psi} \right]$$

$$\frac{\Delta}{(T_{++} + T_{+-})} = \frac{1}{2} \left[1 + \frac{(\bar{\Gamma}_{++} - \bar{\Gamma}_{+-})}{(\bar{T}_{++} + \bar{T}_{+-})} e^{j\psi} \right]$$

These can be reduced to the following forms:

$$\frac{\Sigma}{N_S} = \frac{1}{2} \left(1 + K_S \, e^{j\delta_S} e^{j\psi} \right) \qquad\qquad (18)$$

$$\frac{\Delta}{N_D} = \frac{1}{2} \left(1 - K_D \, e^{j\delta_D} e^{j\psi} \right) \qquad\qquad (19)$$

Where:

$N_S = \Gamma_{++} - \Gamma_{+-}$ = Sum normalization factor

K_S = Sum amplitude unbalance

δ_S = Sum phase unbalance

$N_D = T_{++} + T_{+-}$ = Difference normalization factor

K_D = Difference amplitude unbalance

δ_D = Difference phase unbalance.

The computer was programmed to calculate the values of Σ and Δ as a function of hybrid parameters and to calculate the N, K and δ values defined above. The N values are used in the general mathematical model to calculate the true values of Σ and Δ for various values of ψ.

39

4.2 WORST CASE COMPARATOR PERFORMANCE - NARROW BEAM COMPARATOR

Inspection of the admittance ratio tables in section 3.4 show that for Hybrid A, the maximum ratio is Max Y_3/Min Y_1 = 0.77039829 for the minimum capacity case. Since the analysis assumes equal values of Y_1, the smallest ratio with Min Y_1 in the minimum capacity case is selected and is Min Y_2/Min Y_1 = 0.67158234. The minimum ratio is Min Y_2/Max Y_1 = 0.65235058 for the maximum capacity case. The corresponding maximum ratio is Max Y_3/Max Y_1 = 0.75003719. These two sets of numbers were used in the computer program and the former pair showed slightly worse performance, so they were chosen as representing the worst case values of admittance ratios for Hybrid A. For Hybrids B, C and D it is obvious that the ratio Max Y_2/Min Y_1 = 0.76167924 is the highest and worst admittance ratio, so this value is used for Hybrids B, C and D. The following results include the effect of angle tolerance buildup.

4.2.1 Ideal Hybrid, Ambient Temperature

The values of N, K and δ for the perfect hybrid are as follows:

$$N_S = -j\sqrt{2} = 1.4142135\, e^{-j90^\circ} \qquad N_D = -j\sqrt{2} = 1.4142135\, e^{-j90^\circ}$$

$$K_S = 1.0000000 \qquad\qquad K_D = -1.0000000$$

$$\delta_S = 0^\circ \qquad\qquad\qquad \delta_D = 0^\circ$$

4.2.2 Hybrid A, Ambient Temperature

For $Y_A = 0.67158234$, $Y_B = 0.77039829$, $f_o = 2106$ MHz:

$N_S = 1.3139579 \, e^{-j89.471^\circ}$ $\qquad$ $N_D = 1.5071769 \, e^{-j89.225^\circ}$

$K_S = 1.1470511$ $\qquad\qquad\qquad$ $K_D = -0.87179972$

$\delta_S = 0.246^\circ$ $\qquad\qquad\qquad\qquad$ $\delta_D = 0.246^\circ$

4.2.3 Hybrids B and D, Ambient Temperature

For $Y_A = Y_B = 0.76167924$, $f_o = 2106$ MHz:

$N_S = 1.4103644 \, e^{-j89.471^\circ}$ $\qquad$ $N_D = 1.4102592 \, e^{-j89.207^\circ}$

$K_S = 0.99992544$ $\qquad\qquad\qquad$ $K_D = -1.000072$

$\delta_S = 0.264^\circ$ $\qquad\qquad\qquad\qquad$ $\delta_D = 0.264^\circ$

4.2.4 Hybrid C, Ambient Temperature

For $Y_A = Y_B = 0.76167924$, $f_o = 2193$ MHz:

$N_S = 1.4157993 \, e^{-j84.418^\circ}$ $\qquad$ $N_D = 1.4041833 \, e^{-j81.663^\circ}$

$K_S = 0.99179544$ $\qquad\qquad\qquad$ $K_D = -1.0080139$

$\delta_S = 2.755^\circ$ $\qquad\qquad\qquad\qquad$ $\delta_D = 2.766^\circ$

4.3 TEMPERATURE EFFECTS

As explained in section 3.6.1, the temperature effects are computed by calculating the hybrid performance at the operating frequency using a design frequency corresponding to the dimensional change caused by temperature. The effects of angle tolerance buildup are included in the following results.

4.3.1 Hybrid A at +120°F

For $Y_A = 0.67158234$, $Y_B = 0.77039829$, $f_0 = 2100.2719$ MHz :

$$N_S = 1.314048 \; e^{-j90.877°} \qquad\qquad N_D = 1.5070786 \; e^{-j91.285°}$$

$$K_S = 1.1468976 \qquad\qquad\qquad K_D = -0.87191464$$

$$\delta_S = -0.408° \qquad\qquad\qquad\qquad \delta_D = -0.408°$$

4.3.2 Hybrid A at -85°F

For $Y_A = 0.67158234$, $Y_B = 0.77039829$, $f_0 = 2126.4184$ MHz :

$$N_S = 1.3144661 \; e^{-j88.256°} \qquad\qquad N_D = 1.5066214 \; e^{-j87.445°}$$

$$K_S = 1.146185 \qquad\qquad\qquad K_D = -0.87244888$$

$$\delta_S = 0.811° \qquad\qquad\qquad\qquad \delta_D = 0.812°$$

4.3.3 Hybrids B & D at 120°F

For $Y_A = Y_B = 0.76167924$, $f_0 = 2100.2719$ MHz :

$$N_S = 1.4104517 \; e^{-j90.877°} \qquad\qquad N_D = 1.4101629 \; e^{-j91.315°}$$

$$K_S = 0.99979522 \qquad\qquad\qquad K_D = -1.000198$$

$$\delta_S = -0.438° \qquad\qquad\qquad\qquad \delta_D = -0.438°$$

4.3.4 Hybrids B & D at -85°F

For $Y_A = Y_B = 0.76167924$, $f_0 = 2126.4184$ MHz :

$$N_S = 1.4108575 \; e^{-j88.256°} \qquad\qquad N_D = 1.4097154 \; e^{-j87.385°}$$

$$K_S = 0.99919048 \qquad\qquad\qquad K_D = -1.0007834$$

$$\delta_S = 0.871° \qquad\qquad\qquad\qquad \delta_D = 0.871°$$

4.3.5 Hybrid C at +120°F

For $Y_A = Y_B = 0.76167924$, $f_o = 2187.04$ MHz:

$$N_S = 1.4134573 \, e^{-j85.789°} \qquad N_D = 1.4068239 \, e^{-j83.700°}$$

$$K_S = 0.99530698 \qquad K_D = -1.0045639$$

$$\delta_S = 2.090° \qquad \delta_D = 2.095°$$

4.3.6 Hybrid C at -85°F

For $Y_A = Y_B = 0.76167924$, $f_o = 2214.2505$ MHz:

$$N_S = 1.4183375 \, e^{-j83.222°} \qquad N_D = 1.4012822 \, e^{-j79.898°}$$

$$K_S = 0.98797517 \qquad K_D = -1.011802$$

$$\delta_S = 3.324° \qquad \delta_D = 3.344°$$

4.4 WIDE BEAM COMPARATOR

All hybrids in the wide beam comparator are identical to Hybrids B and D in the narrow beam comparator, so those results apply to all the wide beam hybrids.

4.5 DIODE PHASE SHIFTER (ESTIMATED)

At the input to Hybrid D, the estimated maximum amplitude unbalance is 0.185 db and the estimated maximum phase unbalance is 14° due to manufacturing and tolerance effects on the diode phase shifter. The errors attributed to temperature variation of the phase shifter are negligible. These estimates are for both the narrow beam and wide beam comparators.

4.6 PRECOMPARATOR PHASE SHIFT

As calculated in section 3.6.7, the precomparator differential phase shift due to temperature differences of the feed lines is 6.85° for the narrow beam array and 0.411° for the wide beam array.

REFERENCES

1. Reed, J. and Wheeler, G. J., _A Method of Analysis of Symmetrical Four Port Networks_, IRE Trans. MTT-4, 246-252(1956).

2. Cohn, S., _Problems in Strip Transmission Line_, IRE Trans. MTT-3, 119-124(March, 1955).

3. North American Aviation, Internal Letter from J. Sims to H. Williams, Ref 446A203, dated: May 14, 1968.

4. Osborn, J. D., "CSM-HGA Interchangeability Study-Antenna and RF Circuitry Analysis," TRW Systems Report Number 11176-H080-RO-00, 2 December 1968.